Vacuum 180 (2020) 109458

Contents lists available at ScienceDirect

Vacuum

journal homepage: http://www.elsevier.com/locate/vacuum

A novel hydrothermal induced $BiVO_4/g\text{-}C_3N_4$ heterojunctions visible-light photocatalyst for effective elimination of aqueous organic pollutants

V. Rathi [a], A. Panneerselvam [b,*], R. Sathiyapriya [c]

[a] Department of Physics, Vivekanandha College of Technology for Women, Namakkal, 637205, Tamilnadu, India
[b] Department of Physics, Vivekanandha College of Engineering for Women (Autonomous), Elayampalayam, Tiruchengode, 637205, Tamilnadu, India
[c] Department of Physics, Mahendra Engineering College, Namakkal, 637503, Tamilnadu, India

ARTICLE INFO

Keywords:
$BiVO_4/g\text{-}C_3N_4$
Hydrothermal
Catalyst
4-Chlorophenol
Visible light

ABSTRACT

In this report, a novel $BiVO_4/g\text{-}C_3N_4$ heterojunction photocatalysts were developed through facile and one step hydrothermal route. Various characterization techniques such as X-ray diffraction (XRD), Scanning electron microscope (SEM), Transmission electron microscope (TEM), Raman, UV–Visible diffuse reflectance (UV-DRS), Photoluminescence and Brunauer-Emmett-Teller (BET) analysis have been carried out to know the structural, optical and textural behavior of the pure $BiVO_4$ and various $BiVO_4/g\text{-}C_3N_4$ hybrid catalysts. The basic characterization results suggest that interaction between $BiVO_4$ and $g\text{-}C_3N_4$ was confirmed and a heterojunction was formed on the surface of $g\text{-}C_3N_4/BiVO_4$ composite, which enhanced the separation and transfer of photogenerated electron-hole pairs. Visible light induced photocatalytic degradation test was carried out for all the synthesized catalysts towards rhodamine B (RhB) and 4-chlorophenol (4-CP) dyes. Among the various composite catalysts, the 3:1 mass ratio of $BiVO_4/g\text{-}C_3N_4$ (BVG3) catalyst achieves the optimum photocatalytic activity for the degradation of 4-CP, and reached 95.%, which is 3.7 times better than bare $BiVO_4$ (25%). The hybrid catalyst has also delivered a high apparent constant (0.0821 min^{-1}) and huge stability (loss only 2.25%). The improved photocatalytic mechanism was also discussed.

1. Introduction

In later years, fuel asset deficiency and environmental pollution have ended up imperative issues, and these issues are becoming increasingly noticeable, which makes numerous analysts devote to discover and create modern clean energy. As the representative of the natural neighborly catalyst since of the clean and adequate sunlight as catalytic light source, the semiconductor photocatalytic materials make them encourage be found and adjusted to deliver full play to their characteristics and stimulate their potential application value [1–8]. In recent years, a huge sum of effluents containing various organic poisons such as antimicrobials, drugs, colors, phenolic pollutants and agrochemicals have been discharged into water sources, resulting in genuine natural contamination, which has gotten to be an urgent issue to be solved [9–11]. At display, there are many ways of treating natural pollutants, counting adsorption, micro electrolysis, biological filtration, and the like. In any case, these traditional treatment strategies are complicated and not effective in purification of water. Photocatalytic debasement of toxins based on semiconductors has pulled in significant intrigued [12–14], as a green and proficient strategy for corrupting natural pollutants. Even though, the major challenge in customary process is the restriction in efficiency of solar efficiency within the visible region or insufficient carrier partition capacity [14,15]. To address this issue, incredible exertion has been given to the investigation and preparation of novel photocatalysts for extending the energy utilization to the visible range of the solar spectrum and decreasing the recombination of the photogenerated electron-hole sets [16–19].

Recently, Bismuth-based materials (e.g., Bi_2WO_6, $BiVO_4$, $Bi_2O_2CO_3$) have pulled in supported consideration due to their numerous points of interest, such as prevalent photocatalytic movement under UV and obvious light illumination, special layered structures and resistance to photo corrosion, chemical stability, low/non-toxicity, and soil plenitude. Among the different bismuth-based semiconductors, $BiVO_4$ has been demonstrated to be a perfect photocatalytic fabric for the corruption of natural toxins under visible light irradiation due to its limit band hole and great crystallinity. In any case, destitute quantum yield and destitute visible light assimilation effectiveness are still extraordinary challenges to upgrade the photocatalytic efficiency of bare $BiVO_4$ to

* Corresponding author.
E-mail address: panneer.phy@gmail.com (A. Panneerselvam).

https://doi.org/10.1016/j.vacuum.2020.109458
Received 30 March 2020; Received in revised form 14 April 2020; Accepted 10 May 2020
Available online 10 July 2020
0042-207X/© 2020 Elsevier Ltd. All rights reserved.

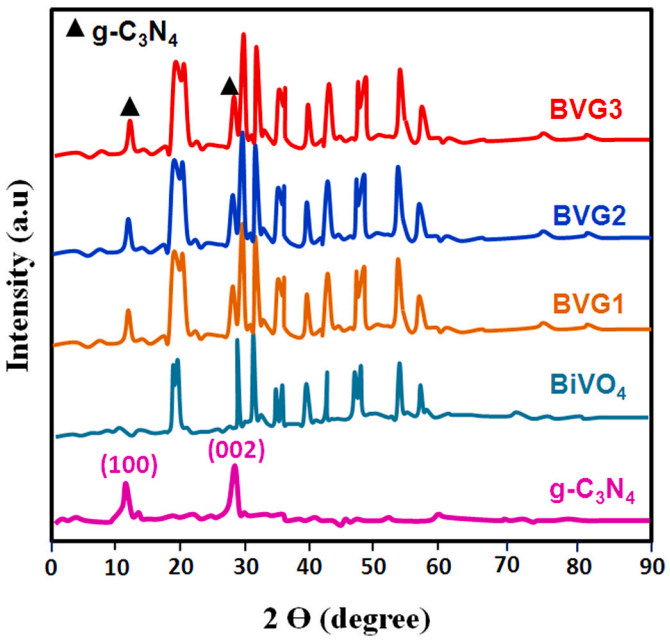


Fig. 1. Powder X-ray diffraction pattern of pure g-C_3N_4, $BiWO_4$ and various composite samples.

meet the commonsense application necessities [20]. To rectify this problem combination with carbon materials especially, Graphitic carbon nitride (g-C_3N_4) has gained amazing acceptance as a visible-light-driven photocatalyst with a distinctive 2D structure and great stability [21,22]. Moreover, the energy levels of g-C_3N_4 and $BiVO_4$ are well matched overlapping band-structures (both of the valence and construction band levels of $BiVO_4$ is lower than that of g-C_3N_4 which make it highly possible to form $BiVO_4$ doped g-C_3N_4 heterojunction with excellent transfer and separation ability of electron-hole pairs in the heterojunction structure [23]. The main objective of this study is to prepare $BiVO_4$/g-C_3N_4 hybrid catalysts via facile hydrothermal technique and study the textural, morphological and optical properties through various basic characterization techniques. The optimum mass ratio of $BiVO_4$ (15 wt%) to g-C_3N_4 show outstanding degradation efficiency, kinetic parameters and stability towards 4-CP under visible light irradiation. To the best of our knowledge, this is first report of high degradation efficiency of 4-CP using $BiVO_4$/g-C_3N_4 hybrid catalysts synthesized by facile hydrothermal route.

2. Experimental procedure

2.1. Materials

Melamine ($C_3H_6N_6$, 99%) was used in this study as a carbon nitride precursor. Bismuth nitrate pentahydrate ($Bi(NO_3)_3{\cdot}5H_2O$), vanadyl acetylacetonate ($C_{10}H_{14}O_5V$), sodium hydroxide (NaOH), rhodamine B (RhB) and 4-Chlorophenol (4-CP) solutions were purchased from Alfa Aesar company (Japan) with purity of 99%. Chemicals were used any further sanitization.

2.2. Preparation of g-C_3N_4, $BiVO_4$ and $BiVO_4$/g-C_3N_4 nanocomposites

Bare g-C_3N_4 was synthesized from Melamine, which is direct annealing of 400 °C for 2 h in air environment [24]. A facile hydrothermal route was used to prepare the $BiVO_4$ nanoparticles. Initially, 1.2 g of $Bi(NO_3)_3{\cdot}5H_2O$ and 0.5 g of $C_{10}H_{14}O_5V$ were mixed with 50 ml of DI water under vigorous stirring of 30 min. Subsequently, the concentrated NaOH solution was added into the above solution to adjusting the pH value to reaches to 8. The resultant suspension was transferred into a Teflon-lined stainless steel autoclave and heated to 150 °C and kept for 12 h, and then cooled down naturally. The pale yellow solid was sequentially washed with water, ethanol, and acetone (20 ml of each) and dried in a desiccator under low vacuum (approx. 10^{-2} mbar) for 24 h and dried at 80 °C overnight. The as synthesize samples was annealed at 300 °C for 4 h in air to improve the crystalline nature of the sample. The final product is pure $BiVO_4$ nanopowders. The g-C_3N_4/$BiVO_4$ photocatalysts were prepared through several steps. First, an appropriate amount of g-C_3N_4 was added into methanol to be ultrasonically stirred for 1 h to completely disperse the g-C_3N_4. Then, the $BiVO_4$ power was added into the g-C_3N_4 suspension and magnetically stirred in a fume hood until solvent evaporation was completed. The g-C_3N_4/$BiVO_4$ composite photocatalysts with different g-C_3N_4 mass ratios were obtained after drying at 80 °C and then calcinating at 300 °C for 4 h to provide enough thermal energy to achieve an interaction between $BiVO_4$ and g-C_3N_4 samples, which could provide a favorable condition for charge transfer from one particle to the other via the interfaces. The mass ratios of the resulting samples were as follows: g-C_3N_4:$BiVO_4$ = 1:1, 2:1, and 3:1. The composites with these different mass ratios were denoted here as BVG1, BVG2 and BVG3, respectively.

2.3. Characterization techniques

Bruker D8 diffractometer with Cu Kα radiation (λ = 1.5418 Å) was used to analysis the structural nature of the samples. The microstructure and elemental composition of the samples were analyzed by using scanning electron microscope (JEOL Model JSM - 6390LV), transmission electron microscope (TEM, H-600-II, Hitachi) and energy dispersive spectra (EDS) (JEOL Model JED – 2300) analysis. The fundamental vibration modes of the samples were measured by Fourier transforms infrared spectroscopy (FT-IR, Nicolet Nexus 470). The specific surface areas and porous nature of materials were further investigated by nitrogen adsorption/desorption measurements on nova 2200e. BRUKER RFS 27: spectrometer and Perkin- Elmer lambda 950 UV–vis.-NIR spectrophotometer was utilized to identify the vibration mode and optical nature of the products.

2.4. Photocatalytic assembly

A glass type photo-reactor which is consists of 500 ml capacity with dimension of 15 cm diameter and 20 cm height. Xenon lamp XQ-500 W with an intensity of 40 mW/cm^2 has been used as the source of visible light to activate the photocatalytic reaction. Initial concentration of the solution consists of 10 mg of catalyst powders with mixed with 50 ml of dyes (20 mg L^{-1}) and stirred for about 30 min to accomplish the adsorption-desorption equilibrium. The absorption ability of rhodamine B (RhB) and 4-chlorophenol (4-CP) dyes were monitored using UV–Vis–NIR spectrophotometer (UV-2600SHIMADZU) with the corresponding wavelength of 540 and 220 nm, respectively. The visible light activation time is varied from 0 to 100 min with optimum interval of 20 min the degradation efficiency and first order kinetics was calculated from the previous works [25,26].

3. Results and discussion

3.1. Powder X-ray diffraction (XRD) analysis

The structural perfection of the prepared catalysts was obtained through powder XRD method. Fig. 1 shows the powder XRD pattern of g-C_3N_4, $BiVO_4$ and various heterostructure composite samples, respectively. There are two typical diffraction peaks were positioned at 2θ value of 11.1 and 27.5° is index to the (100) and (002) orientation plane, which originate from the interlayer stacking of aromatic segments of bare g-C_3N_4 [27]. The monoclinic structure of bare $BiVO_4$ sample is gotten through their diffraction patterns. All the sharp diffraction patterns without g-C_3N_4 peaks in the bare $BiVO_4$ sample is denoted that

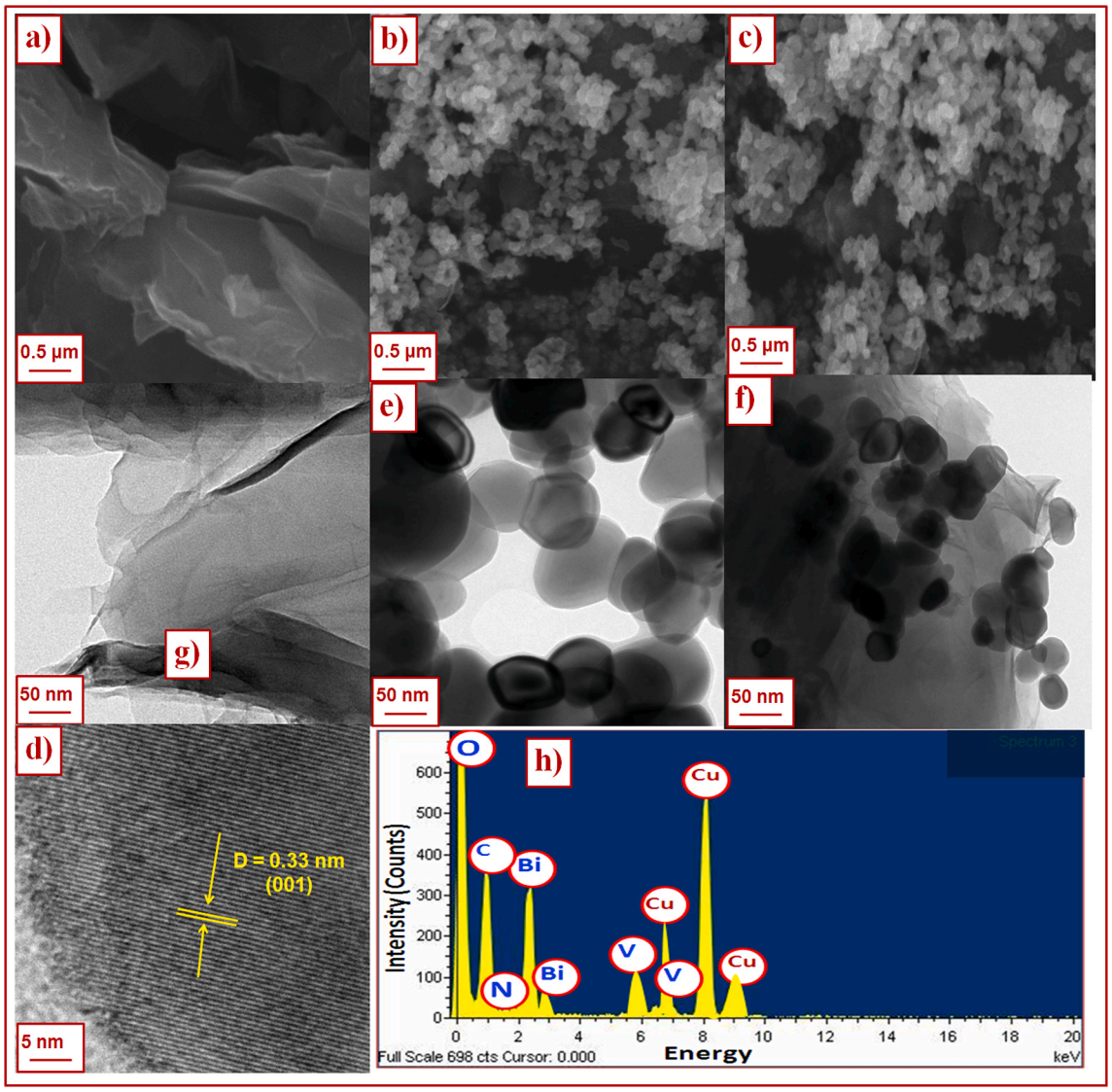


Fig. 2. SEM images of **a)** g-C_3N_4; **b)** $BiVO_4$; **c)** BVG3; TEM images of **d)** g-C_3N_4; **e)** $BiVO_4$; **e)** BVG3; **g)** HRTEM image of BVG3; **h)** EDAX spectra of BVG3.

high crystalline nature with monoclinic structure and the results are matched perfectly with the standard value (JCPDS card No. 14-0688). The existence of $BiVO_4$ and g-C_3N_4 related orientation in the all the composite samples are illustrated that formation of composite structure. It was noticed that intensities of the composite samples are very sharp that bare catalysts sample. This could be due to the high crystalline nature and was further verified their crystalline size calculated from the Scherrer's equation [28] and found to be 27, 33, 39, 45 and 51 nm for g-C_3N_4, $BiVO_4$, BVG1, BVG2 and BVG3 catalysts, respectively.

3.2. SEM, TEM, HRTEM with EDAX analysis

Information about the morphological feature of the catalysts samples were analyzed through SEM and TEM images. Fig. 2(a–c) SEM images of the g-C_3N_4, $BiVO_4$, BVG3 samples, respectively. SEM image of pure g-C_3N_4 displays a sheet-like morphology with a smooth surface (Fig. 2a). The irregular spherical shaped nanoparticles are found in the bare $BiVO_4$ sample (Fig. 2b), the particles were enveloped on the surface of the g-C_3N_4 sheets in the composite sample (Fig. 2c). Also, the TEM image (Fig. 2d) has shown that g-C_3N_4 is almost transparent, indicating its few-layer structure. Obvious stacked pore structure was found between the sheets. The bare $BiVO_4$ nanoparticles (Fig. 2e) are warped throughout the g-C_3N_4 sheets in the composite sample (Fig. 2f). Well defined lattice fringes can be seen in the high resolution TEM image, with the fringe spacing being d = 0.33 nm, which is (001) plane of monoclinic structure BiVO4 (Fig. 2g). Fig. 2h) shows the EDAX image of BVG3 sample, which is mainly, exposed to the major elements of Bi, V, O, C and N. The presence of C and N elements in the image again supported that the g-C_3N_4 was successfully incorporated in the $BiVO_4$ crystal matrix.

3.3. FTIR analysis

The chemical bonding of the synthesized catalysts were evaluated using FTIR. Fig. 3 shows the FTIR spectra of all the catalyst powders, which is measured with wide range wavenumber (4000-400 cm^{-1}). The C═N and C–N stretching vibrations of g-C_3N_4 is positioned in the range of 900–1100 cm^{-1} [29]. There are two major vibrations are located at 745 and 841 cm^{-1} for bare $BiVO_4$ sample. This could be attributed to the asymmetric stretching vibration of $\nu 3$ (VO_4) and symmetrical stretching vibration of $\nu 1$(VO_4) [30]. The bare g-C_3N_4 sample show series of stretching mode of the N–H bond, peaks at 1555 cm^{-1}, 1455 cm^{-1}, 1318 cm^{-1} and 1244 cm^{-1} are ascribed to the vibration absorption of the heptazine ring heterocyclic compound [31]. It was clearly noted that co-existence of g-C_3N_4 vibrations (1500-1300 cm^{-1}) along with $BiVO_4$ in the composite sample (BVG2 and BVG3) is further supported that g-C_3N_4 is successfully decorated in the $BiVO_4$. It was clearly noted that the

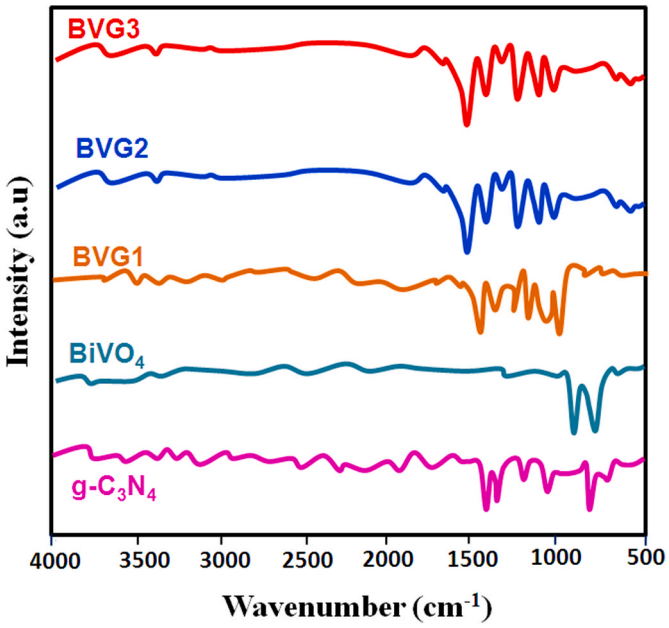


Fig. 3. FTIR spectra of pure g-C_3N_4, $BiVO_4$ and various composite samples.

vibration bands of g-C_3N_4 is not detected in the bare $BiVO_4$ sample. These vibration Interestingly, characteristic peak of the s-triazine ring in the composite shifts slightly to the high wavelength direction (~815 cm^{-1}), indicating that there was an interaction between 2D g-C_3N_4 and $BiVO_4$, which on one hand proves the successful preparation of the 2D g-C_3N_4/$BiVO_4$ composite.

3.4. UV–Vis DRS analysis

The optical absorption and band gap energies are estimated from the UV–Vis DRS analysis. Fig. 4a) shows the UV absorption spectra of the all the catalyst powders. The optical absorption was found in the UV region for both bare g-C_3N_4 and $BiVO_4$ samples, respectively. After incorporation of g-C_3N_4 in to $BiVO_4$, the optical absorption edges were significantly transferred to the visible region. The absorption is all the composite samples are in the visible region. Especially, the BVG3 sample exhibits highest shift in the longer wavelength in the absorption edge. The results suggest that the composite samples are more absorption nature in the visible light and absorb more photons on its catalyst surface, which is beneficial for improving their photocatalytic performance. A considerable longer shift of the composite sample denoted that decreasing the optical band gap energy and was further estimated by K-M model [32,33]. The optical band gap energies are 3.35, 3.08, 2.94, 2.71 and 2.48 eV for g-C_3N_4, $BiVO_4$, BVG1, BVG2 and BVG3 catalysts, respectively.

3.5. Photoluminescence spectra analysis

Fluorescence intensity of catalyst is very important to determine the charge separation efficiency of the electron-hole pairs of the photocatalyts. Hence, room temperature photoluminescence study was taken for all the catalyst samples using He–Ne as laser source with excitation wavelength of 350 nm (Fig. 5). All the catalyst samples exposed the broad emission in the visible region (400-450 nm). It is obvious that the fluorescence intensity of 15 wt% $BiVO_4$ loaded g-C_3N_4 is significantly lower than that of pure g-C_3N_4 and $BiVO_4$, which means that the

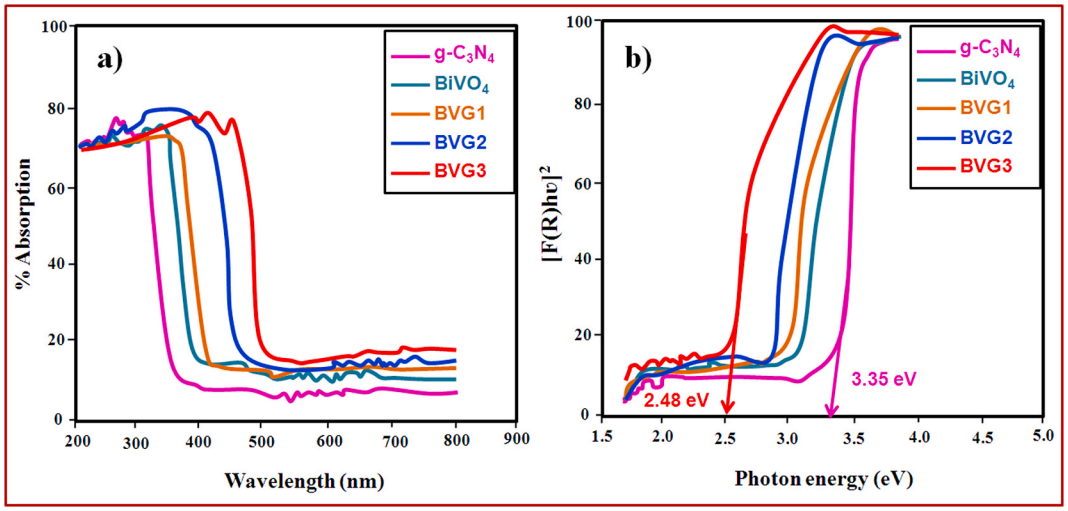


Fig. 4. UV–Vis DRS spectra of pure g-C_3N_4, $BiVO_4$ and various composite catalystsa) Absorption spectra **b)** Kubelka-Munk model.

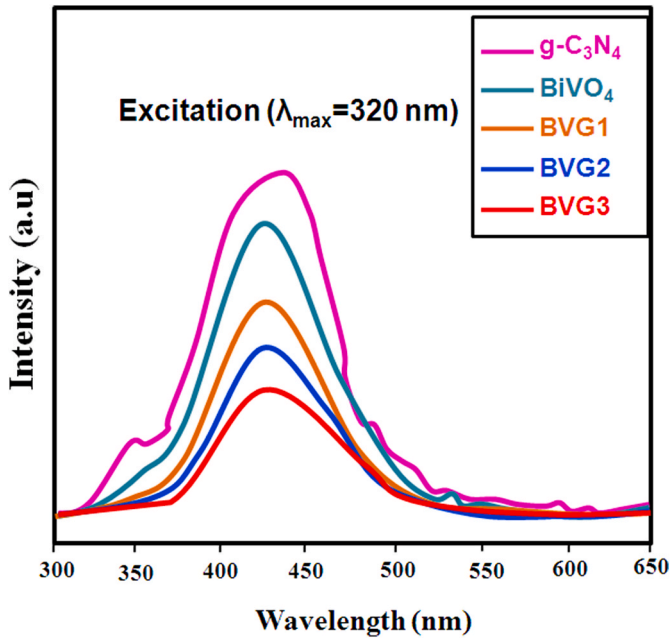


Fig. 5. Photoluminescence spectra of pure g-C_3N_4, $BiVO_4$and various composite samples.

recombination probability of photogenerated electrons and holes in $BiVO_4$/g-C_3N_4 (BVG3) catalyst is lower than that of pure g-C_3N_4 and $BiVO_4$. This behavior is beneficial for improving the photocatalytic performance for the composite samples.

3.6. Nitrogen adsorption and desorption analysis

Agreeing to past reports, the particular surface region of photocatalyst is an critical factor influencing the productivity of photocatalytic degradation, since the measure of the particular surface region directly influences the number of photocatalyst active sites and adsorption action [34,35]. Hence, N_2 adsorption-desorption measurement was taken and relevant plot is shown in Fig. 6a). The spectra illustrate that cleat type IV isotherm with H3 hysteresis loop, which denoted that mesoporous nature of the samples [36]. The BET surface area and BJH pore size was found to be 84.5 m^2/g and 27.5 nm for BVG3 catalyst, which is higher than bare $BiVO_4$ catalyst (surface area = 51.4 m^2/g and pore size = 46.5 nm). From the results, g-C_3N_4 alters within the particular surface regions of the $BiVO_4$ photo catalysts, which is favorable to enhancing the photocatalytic performance.

3.7. Photocatalytic studies

3.7.1. UV absorption characteristics

In this work, RhB and 4-CP pollutants were chosen to evaluate the photocatalytic activity of the catalyst powders. Initially, absorption ability of the catalysts was evaluated using RhB and 4-CP dyes with equivalent wavelength of 540 and 220 nm, respectively. UV–Vis–NIR spectrophotometer (UV-2600SHIMADZU) was carried out to monitored the absorption characteristics of the catalysts and the relevant plot is

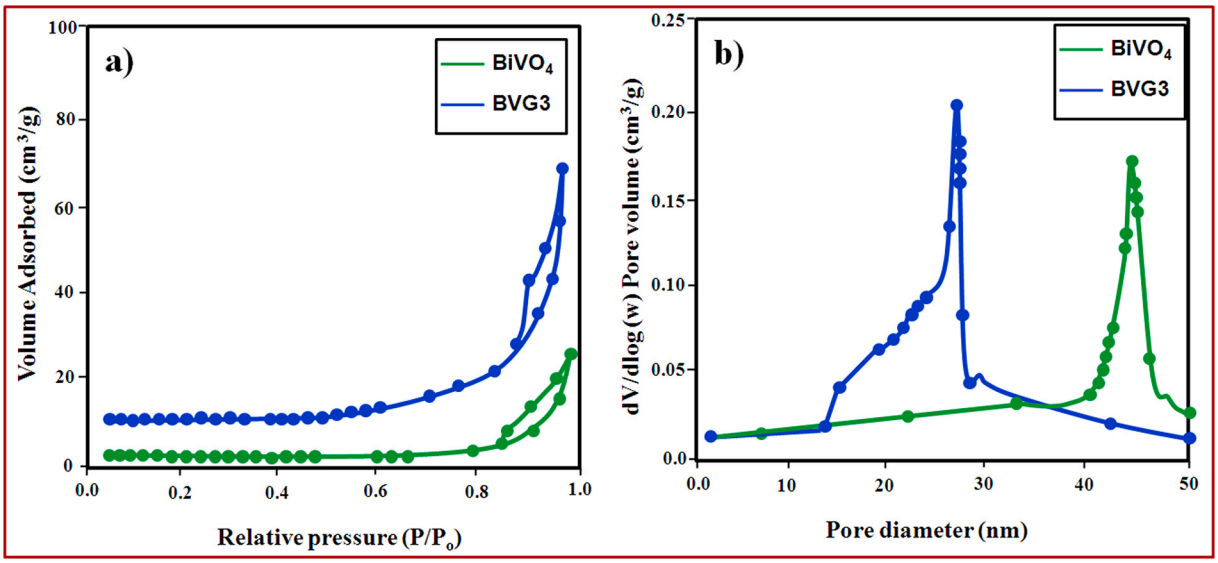


Fig. 6. a) N_2 adsorption and desorption analysis $BiVO_4$ and BVG3 samplesb) corresponding pore size distribution.

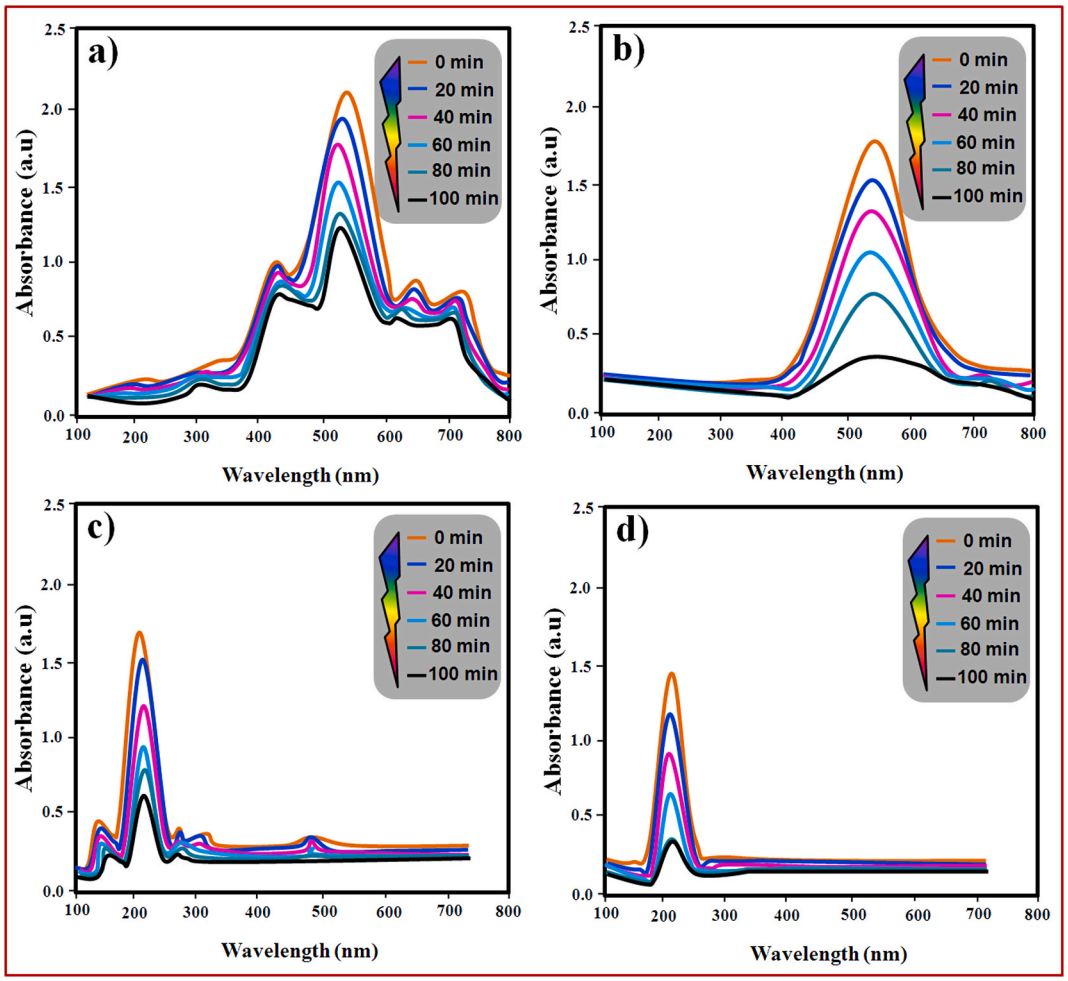


Fig. 7. UV absorption spectra of RhB using **a)** $BiVO_4$; **b)** BVG3; UV absorption spectra of 4-CP using **c)** $BiVO_4$; **d)** BVG3 under different illumination time.

depicts in Fig. 7(a–d). The maximum absorption edge of the catalysts were started to decrease with the increase of the visible light illuminations. The absorption intensity was totally vanish with the illumination time is reached to 100 min testing. The results demonstrate that the obtained catalysts are more energetic under visible light and they were used as degradation of different organic pollutants under visible light irradiation.

3.7.2. Degradation test

Degradation of pollutants was further examined for both dyes and the temporal degradation profile is shown in Fig. 8 (a&b). Initially, Firstly, the dark adsorption equilibrium was recognized earlier to the visible irradiation, and all of the solutions show nearly unchanged concentration after stirring for 30 min the bare $BiVO_4$ catalyst exhibits low degradation efficiency of 29 and 37% towards RhB and 4-CP dyes under visible light illumination. This may ascribed to the rapid recombination of photo-generated electron-hole pairs. When the $BiVO_4$ is loaded in to g-C_3N_4 the significant improved was observed in the photo degradation efficiency. The maximum degradation is achieved by BVG3 catalysts for both dyes and estimated to be 95 and 89% for RhB and 4-CP dyes, respectively. This is mainly the following reasons (i) rapid generation of electron-hole pair (ii) suppress the recombination rate of electron-hole pairs (iii) high surface area and (iv) huge absorption visible light on the catalyst surface during the photocatalytic reaction.

3.7.3. Kinetic study

Degradation performance of the catalysts was further scrutinizing the first order kinetic relation [37] and the resultant graph is shown in Fig. 8 (c & d). The apparent constant (k) of RhB and 4-CP dyes are 0.0821 min^{-1} and 0.0563 min^{-1}, which is 3.5 times (0.0231 min^{-1}) and 2.7 times (0.0215 min^{-1}) better than bare $BiVO_4$ catalyst. Based on the photocatalytic results the photocatalytic parameter values are estimated and summarized in Table 1. Among the various composite catalysts, the 3:1 mass ratio of $BiVO_4$/g-C_3N_4 (BVG3) catalyst show outstanding degradation efficiency towards RhB and 4-CP dyes. This behavior was further confirmed through the variation in their composites ratio. Further the ratio of g-C_3N_4:$BiVO_4$ is adjust to 4:1 and 5:1 and denoted as BVG4 and BCG5, respectively. The degradation efficiency was found to be 41, 77, 89, 81 and 71 for BVG1, BVG2 BVG3, BVG4 and BVG3 catalysts, respectively (Fig. 8 e&f). The same trend was also obtained in the 4-CP removal efficiency. Hence, the results suggest that the optimum ratio of 3:1 $BiVO_4$/g-C_3N_4 (BVG3) catalyst show outstanding degradation efficiency compared with other composite catalysts. This might be due to the effective prevention of the electron-hole recombination rate of the catalyst. Moreover, the results obtained in the present work are higher than that of previous published $BiVO_4$/g-C_3N_4 heterojunctions [38–42]. The comparison results of the obtained sensor are also shown in Table .2.

3.7.4. COD removal test

The high catalytic efficiency of the obtained catalysts was further evaluated through the monitoring COD removal efficiency both dyes and the results are shown in Fig. 9 (a&b). The results demonstrate that the maximum decolorization efficiency was achieved by BVG3 catalysts, it was found to be 90 and 82% for COD removal efficiency of RhB and 4-CP pollutants.

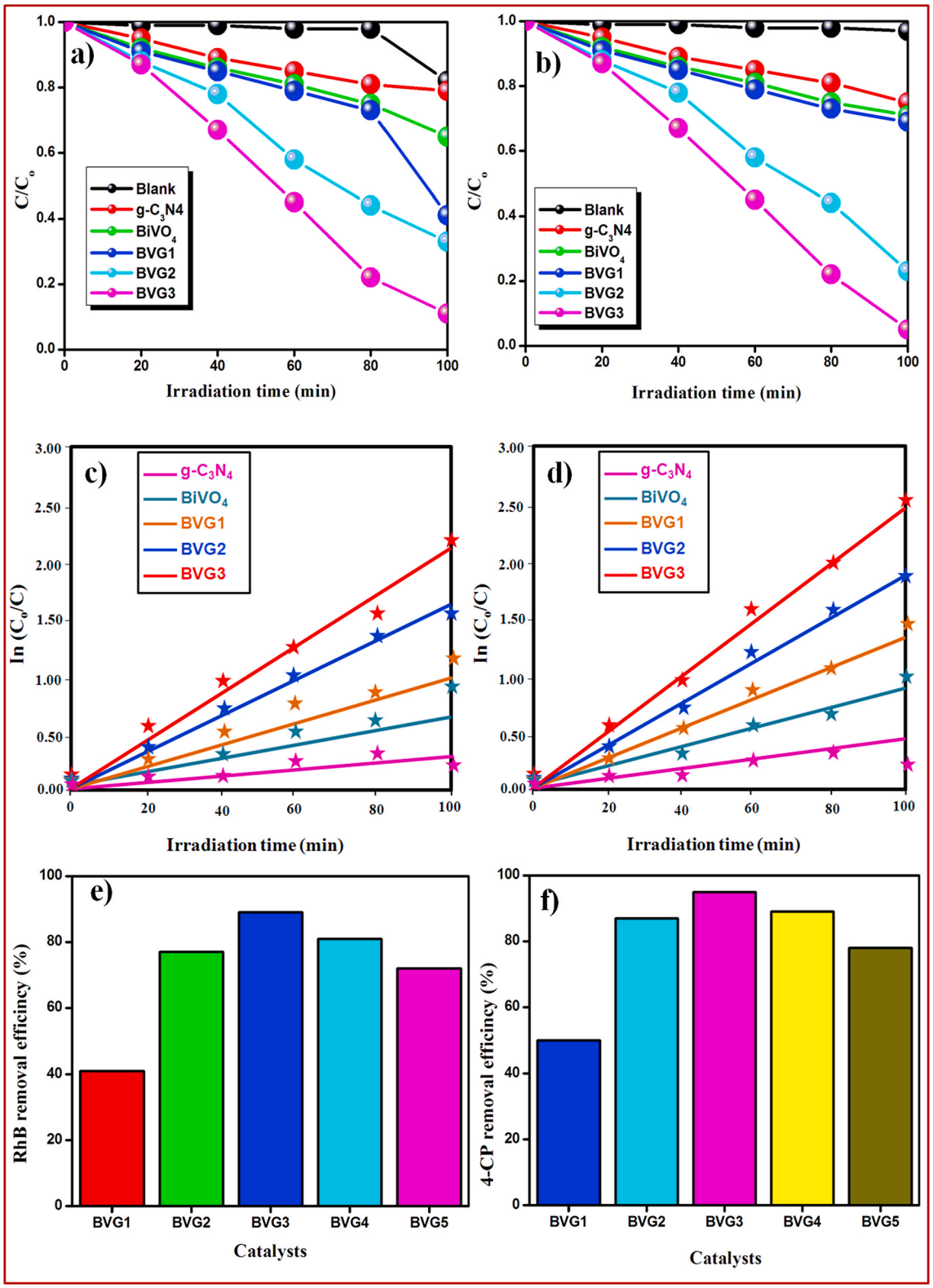


Fig. 8. Temporal degradation profile of **a)** RhB; **b)** 4-CP; Kinetic plot of **c)** RhB; **d)** 4-CP for all the catalyst powders; Degradation efficiency of **e)** RhB; **f)** 4-CP for all the catalyst composite catalysts samples.

Table 1
Photocatalytic parameters of pure g-C_3N_4, $BiVO_4$ and various composite samples.

Samples	Band gap (eV)	Rate constantof RhB		Rate constant of 4-CP		Degradation efficiency at 100 min	
		K (h^{-1})	R^2	K (h^{-1})	R^2	RhB	4-CP
g-C_3N_4	3.35	0.0098	0.955	0.0821	0.961	25	31
$BiVO_4$	3.08	0.0073	0.935	0.0701	0.977	29	37
BVG1	2.94	0.0061	0.922	0.0502	0.948	41	50
BVG2	2.70	0.0193	0.982	0.0348	0.977	77	87
BVG3	2.48	0.0205	0.998	0.0231	0.988	89	95

Table 2
Comparison of RhB degradation efficiency between our results and previous works.

Materials	Light	Dye	Irradiation time (min)	Efficiency (%)	REF
g-C_3N_4/$BiVO_4$	Visible	RhB	120	73.8	[38]
$BiVO_4$@g-C_3N_4	Visible	RhB	80	85.0	[39]
g-C_3N_4/$BiVO_4$	Visible	RhB	120	71.2	[40]
$BiVO_4$/g-C_3N_4	Visible	RhB	120	74.1	[41]
$BiVO_4$/g-C_3N_4	Visible	RhB	60	84.0	[42]
Present work	Visible	RhB	100	89.0	–

3.7.5. Stability test

The stability test was further carried out to know the suitability of the practical device applications of the present catalysts. Fig. 9 (c&d) long term stability test of the catalysts towards RhB and 4-CP dyes under same experimental condition. After five consecutive runs, no obvious deactivation of the composite photocatalyst is observed. Hence, it was concludes that the obtained catalysts were exhibited excellent stability in the visible light photochemical degradation reactions.

3.7.6. Photocatalytic mechanism

Fig. 10 shows the schematic representation of the improved photocatalytic mechanism of the heterojunction catalysts. The results gotten from the photocatalytic results suggest that $BiVO_4$/g-C_3N_4 catalysts show superior performance. This could be due to the equivalent CB and VB bands as well diminish the electron-hole pair recombination between g-C_3N_4 and $BiVO_4$ [43,44]. The electrons are excited from VB to higher energy level of both g-C_3N_4 and $BiVO_4$ under visible light irradiation. These photo-excited electrons are migrate with photo-induced holes further these transfer from $BiVO_4$ VB to g-C_3N_4 VB. Due to this mechanism recombination rate of electron-hole pair is significantly hold back, which results in enhanced photocatalytic performance. Furthermore, g-C_3N_4 has a large specific surface area, a stable two-dimensional conjugated structure, and then more adsorbed contaminants can be collected on the surface of the composite. Due to the lower band gap energy and huge surface area with specific mesoporous nature of the $BiVO_4$/g-C_3N_4 heterostructures may utilize more visible light and

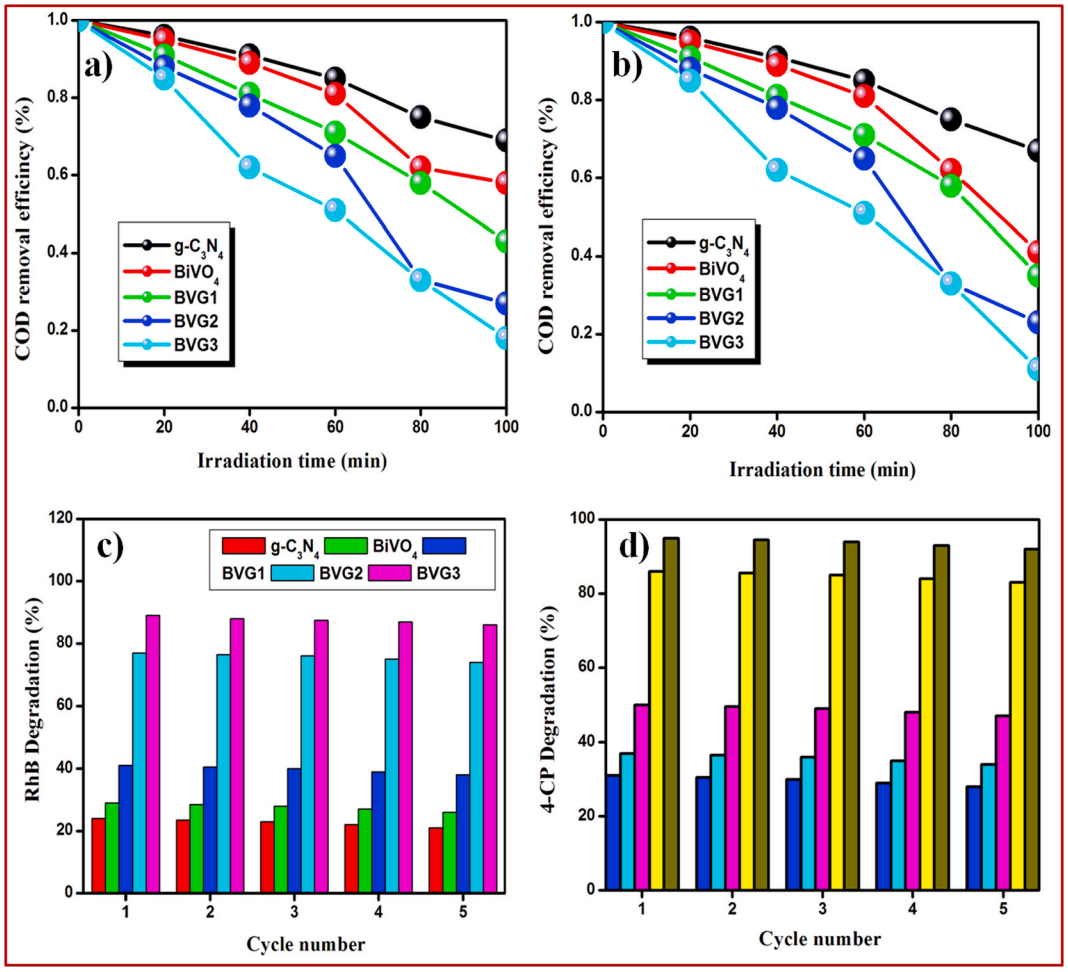


Fig. 9. COD removal efficiency of **a)** RhB; **b)** 4-CP for all the catalysts; cycling stability test of **c)** RhB; **d)** 4-CP pollutants using all the catalyst samples.

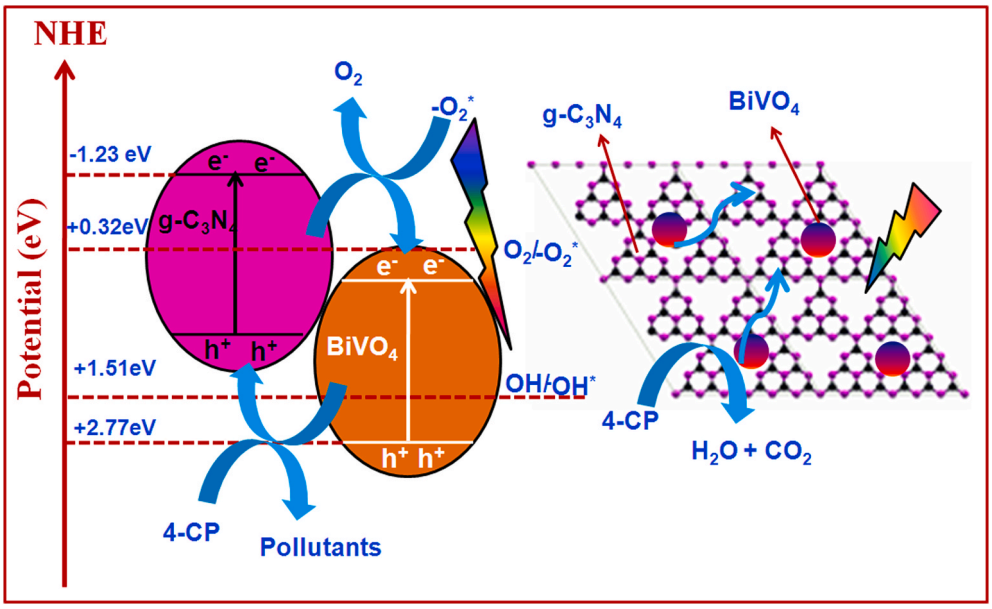


Fig. 10. Schematic representation of the photocatalytic mechanism of the $BiVO_4$/g-C_3N_4 hybrid photocatalyst under visible light irradiation.

decrease the recombination rate of photogenerated carriers [45,46]. Hence, the $BiVO_4$/g-C_3N_4 heterostructures exhibits tremendous photocatalytic performance than compared with bare g-C_3N_4 and $BiVO_4$ catalysts.

4. Conclusions

In summing up, we have rationally developed a 2D multilayered nanostructure photocatalysts with various compositions of $BiVO_4$ and g-C_3N_4 by a one step facile hydrothermal route. The structural, morphological and optical properties of the fabricated catalysts were systematically investigated through XRD, SEM, TEM, UV-DRS, and PL analysis. Among the various composite catalysts, the 3:1 mass ratio of $BiVO_4$/g-C_3N_4 (BVG3) catalyst achieves the optimum photocatalytic activity for the degradation of 4-CP, and reached 95.%, which is 3.7 times better than bare $BiVO_4$ (25%). This can be attributed to two reasons. First, the new heterojunction formed on the interface between g-C_3N_4 (100) and $BiVO_4$, which facilitates the separation of photogenerated electron-hole pairs. Secondly, the mesoporous structure and good interface contact are favorable for the transfer of electrons, thus inhibiting the combination of photogenerated electrons and holes. The photocatalytic mechanism shows that the photocatalytic degradation of RhB is attributed to the effect of the direct oxidation process through h^+ and the oxidation action of the produced $\cdot O_2$ radicals. However, ·OH was determined to be not involved in photocatalytic degradation. Furthermore, the most active 3:1 mass ratio of $BiVO_4$/g-C_3N_4 (BVG3) catalyst exhibits enough catalytic stability, showing great potential as cost-effective heterogeneous visible-light-driven photocatalyst for the purification of aqueous organic pollutants in future applications.

Declaration of competing interest

The authors declare that they have no known competing financial interests or personal relationships that could have appeared to influence the work reported in this paper.

References

[1] Gaurav K Upadhyay, Jeevitesh K. Rajput, Trilok K. Pathak, Vinod Kumara, L. P. Purohit, Synthesis of ZnO:TiO_2 nanocomposites for photocatalyst application in visible light, Vacuum 160 (2019) 154–163.
[2] Tengfei Ma, Jie Bai, Chunping Li, Facile synthesis of g-C_3N_4 wrapping on one-dimensional carbon fiber as a composite photocatalyst to degrade organic pollutants, Vacuum 145 (2017) 47–54.
[3] Yidi Dong, Lei Xing, Ahmad Umar, Xiang Wu, Efficient removal of organic dyes molecules by grain-like α-Fe_2O_3 nanostructures under visible light irradiation, Vacuum 150 (2018) 35–40.
[4] S.G. Maryam, H.Y. Aziz, Fe_3O_4/ZnO/$CoWO_4$ nanocomposites: novel magnetically separable visible-light-driven photocatalysts with enhanced activity in degradation of different dye pollutants, Ceram. Int. 43 (2017) 3063–3071.
[5] G.N. Behrouz, H.Y. Aziz, Ternary ZnO/AgI/Ag_2CO_3 nanocomposites: novel visible-light- driven photocatalysts with excellent activity in degradation of different water pollutants, Mater. Chem. Phys. 184 (2016) 210–221.
[6] Z. Zhu, X. Tang, C. Ma, et al., Fabrication of conductive and high-dispersed Ppy@Ag/g-C_3N_4 composite photocatalysts for removing various pollutants in water, Appl. Surf. Sci. 387 (2016) 366–374.
[7] H. Moriwaki, Y. Akaishi, M. Akamine, H. Usami, Photodegradation of environmental pollutants using perylene adsorbed on silica gel as a visible-light photocatalyst, Appl. Catal. B Environ. 204 (2017) 456–464.
[8] F.J. Chen, Y.L. Cao, D.Z. Jia, A. Luu, Solid-state synthesis of ZnS/graphene nanocomposites with enhanced photocatalytic activity, Dyes Pigments 120 (2015) 8–14.
[9] Y.X. Liu, H.X. Dai, J.G. Deng, L. Zhang, C.T. Au, Three-dimensional ordered macroporous bismuth vanadates: PMMA-templating fabrication and excellent visible light-driven photocatalytic performance for phenol degradation, Nanoscale 4 (2012) 2317–2325.
[10] K.F. Zhang, Y.X. Liu, J.G. Deng, S.H. Xie, H.X. Lin, X.T. Zhao, J. Yang, Z. Han, H. D. Prof, Fe_2O_3/3DOM $BiVO_4$: high-performance photocatalysts for the visible light-driven degradation of 4-nitrophenol, Appl. Catal., B 202 (2017) 569–579.
[11] C.M. Li, Y. Xu, W.G. Tu, G. Chen, R. Xu, Metal-free photocatalysts for various applications in energy conversion and environmental purification, Green Chem. 19 (2017) 882–899.
[12] L. Qin, H.Z. Chen, J. Lei, Y.Q. Wang, T.Q. Ye, H.G. Zheng, Photodegradation of some organic dyes over two metal-organic frameworks especially high efficiency for safranine T, Cryst. Growth Des. 17 (2017) 1293–1298.
[13] W.B. Hou, S.B. Cronin, A review of surface plasmon resonance-enhanced photocatalysis, Adv. Funct. Mater. 23 (2013) 1612–1619.
[14] W.J. Zhou, H. Liu, J.Y. Wang, D. Liu, G.J. Du, J.J. Cui, Ag_2O/TiO_2 nanobelts heterostructure with enhanced ultraviolet and visible photocatalytic activity, ACS Appl. Mater. Interfaces 2 (2010) 2385–2392.
[15] Q. Xiang, J. Yu, M. Jaroniec, Graphene-based semiconductor photocatalysts, Chem. Soc. Rev. 41 (2012) 782–796.
[16] W. Zhao, J.H. Li, Z.B. Wei, S.M. Wang, H. He, C. Sun, S. Yang, The effective photocatalysis and antibacterial properties of AgBr/$AgVO_3$ composites under visible-light, Appl. Catal., B 179 (2015) 9–20.
[17] B. Qiu, M. Xing, J. Zhang, Mesoporous TiO_2 nanocrystals grown in situ on graphene aerogels for high photocatalysis and lithium-ion batteries, J. Am. Chem. Soc. 136 (2014) 5852–5855.
[18] R.C. Pawar, C.S. Lee, Single-step sensitization of reduced graphene oxide sheets and CdS nanoparticles on ZnO nanorods as visible-light photocatalysts, Appl. Catal., B 144 (2014) 57–65.
[19] K.A. Tsai, Y.J. Hsu, Graphene quantum dots mediated charge transfer of CdSe nanocrystals for enhancing photoelectrochemical hydrogen production, Appl. Catal., B 164 (2015) 271–278.

[20] Y. Yan, C. Wang, X. Yan, L.S. Xiao, J.H. He, W. Gu, W.D. Shi, Graphene acting as surface phase junction in anatase–graphene–rutile heterojunction photocatalysts for H2 production from water splitting, J. Phys. Chem. C 18 (2014) 23519–23526.

[21] J. Yi, W. El-Alami, Y. Song, H. Li, P.M. Ajayan, H. Xu, Emerging surface strategies on graphitic carbon nitride for solar driven water splitting, Chem. Eng. J. 382 (2020) 122812.

[22] Y. Song, J. Gu, K. Xia, J. Yi, H. Chen, X. She, Z. Chen, C. Ding, H. Li, H. Xu, Construction of 2D SnS_2/g-C_3N_4 Z-scheme composite with superior visible light potocatalytic performance, Appl. Surf. Sci. 467–468 (2019) 56–64.

[23] M. Mousavi, A. Habibi-Yangjeh, S.R. Pouran, Review on magnetically separable graphitic carbon nitride-based nanocomposites as promising visible-light-driven photocatalysts, J. Mater. Sci. Mater. Electron. 29 (2017) 1719–1747.

[24] S. Prabhu, M. Pudukudy, S. Harish, M. Navaneethan, S. Sohila, K. Murugesan, R. Ramesh, Facile construction of djembe-like ZnO and its composite with g-C_3N_4 as a visible-light- driven heterojunction photocatalyst for the degradation of organic dyes, Mater. Sci. Semicond. Process. 106 (2020) 10454.

[25] M. Arami, N.Y. Limaee, N.M. Mahmoodi, N. Salman, Equilibrium and kinetics studies for the adsorption of direct and acid dyes from aqueous solution by soy meal hull, J. Hazard Mater. 135 (2006) 11–19.

[26] I.K. Konstantinou, T.A. Albanis, TiO_2-Assisted photocatalytic degradation of azo dyes in aqueous solution: kinetic and mechanistic investigations: a review, Appl. Catal., B 49 (2014) 1–14.

[27] H.N. Che, G.B. Che, H.J. Dong, W. Hu, H. Hu, C.B. Liu, C. Liu, Fabrication of Z-scheme Bi_3O_4Cl/g-C_3N_4 2D/2D heterojunctions with enhanced interfacial charge separation and photocatalytic degradation various organic pollutants activity, Appl. Surf. Sci. 455 (2018) 705–716.

[28] M. Parthibavarman, K. Vallalperuman, S. Sathishkumar, M. Durairaj, K. Thavamani, A novel microwave synthesis of nanocrystalline SnO_2 and its structural optical and dielectric properties, J. Mater. Sci. Mater. Electron. 25 (2014) 730–735.

[29] J. Yi, X. She, Y. Song, H. Xu, P. Zhang, Z. Mo, L. Liu, D. Du, H. Li, A silver on 2D white- C_3N_4 support photocatalyst for mechanistic insights: synergetic utilization of plasmonic effect for solar hydrogen evolution, RSC Adv. 6 (2016) 112420–112428.

[30] X. She, J. Yi, Y. Xu, Y. Song, L.i. Huang, H. Ji, H. Xu, H. Li, Designing Z-scheme 2D-C_3N_4/Ag_3VO_4 hybrid structures for improved photocatalysis and photocatalytic mechanism insight, Phys. Status Solidi 214 (2017) 1600946.

[31] J.T. Zhang, F. Huang, Enhanced visible light photocatalytic H_2 production activity of g-C_3N_4 via carbon fiber, Appl. Surf. Sci. 358 (2015) 287–295.

[32] M. Parthibavarman, S. Sathishkumar, S. Prabhakaran, M. Jayashree, R. BoopathiRaja, High visible light-driven photocatalytic activity of large surface area Cu doped SnO_2 nanorods synthesized by novel one-step microwave irradiation method, J. Iran. Chem. Soc. 15 (2018) 2789–2801.

[33] M. Parthibavarman, M. Karthik, P. Sathishkumar, R. Poonguzhali, Rapid synthesis of novel Cr-doped WO_3 nanorods: an efficient electrochemical and photocatalytic performance, J. Iran. Chem. Soc. 15 (2018) 1419–1430.

[34] C.X. Li, X.Y. Li, B. Liu, X.Y. Wang, G.B. Che, X. Lin, A novel Ag_3PO_4/Ag/$Ag_2Mo_2O_7$ nanowire photocatalyst: ternary nanocomposite for enhanced photocatalytic activity, Chin. J. Chem. Phys. 31 (2018) 92–98.

[35] H.N. Che, L.H. Liu, G.B. Che, H.J. Dong, C.B. Liu, C.M. Li, Control of energy band, layer structure and vacancy defect of graphitic carbon nitride by intercalated hydrogen bond effect of NO_3 toward improving photocatalytic performance, Chem. Eng. J. 357 (2019) 209–219.

[36] M. Sumathi, A. Prakasam, P.M. Anbarasan, High capable visible light driven photocatalytic activity of WO_3/g-C_3N_4 hetrostructure catalysts synthesized by a novel one step microwave irradiation route, J. Mater. Sci. Mater. Electron. 30 (2019) 3294–3304.

[37] M. Parthibavarman, S. Sathishkumar, M. Jayashree, R. BoopathiRaja, Microwave assisted synthesis of pure and Ag doped SnO_2 quantum dots as novel platform for high photocatalytic activity performance, J. Cluster Sci. 30 (2019) 351–363.

[38] Chunxue Li, Huinan Che, Chunbo Liu, Guangbo Che, Paul A. Charpentier, William Z. Xu, Xiuyan Wang, Lihui Liu, Facile fabrication of g-C_3N_4 QDs/$BiVO_4$ Z-scheme heterojunction towards enhancing photodegradation activity under visible light, J. Taiwan Instit. Chem. Eng. 95 (2019) 669–681.

[39] Kangdi Zhong, Junwei Feng, Hongbo Gao, Yamin Zhang, Kangrong Lai, Fabrication of $BiVO_4$@g-C_3N_4(100) heterojunction with enhanced photocatalytic visible-light-driven activity, J. Solid State Chem. 274 (2019) 142–151.

[40] Li Li, Mao Mao, Xiaojie She, Jianjian Yi, Minqiang He, Li Pan, Zhigang Chen, Hui Xu, Huaming Li, Direct Z-scheme photocatalyst for efficient water pollutant degradation: a case study of 2D g-C_3N_4/$BiVO_4$, Mater. Chem. Phys. 241 (2020) 122308.

[41] Jie Zhao, Jinghui Yan, Huaijie Jia, Shaowei Zhong, Xinyan Zhang, Lei Xu, $BiVO_4$/g-C_3N_4 composite visible-light photocatalyst for effective elimination of aqueous organic pollutants, J. Mol. Catal. Chem. 424 (2016) 162–170.

[42] Zhichao Sun, Zhiquan Yu, Yingya Liu, Chuan Shi, Mingshan Zhu, Anjie Wang, Construction of 2D/2D $BiVO_4$/g-C_3N_4 nanosheet heterostructures with improved photocatalytic activity, J. Colloid Interface Sci. 533 (2019) 251–258.

[43] F. Chen, Q. Yang, Y. Wang, J.W. Zhao, D.B. Wang, X.M. Li, Z. Guo, H. Wang, Y. C. Deng, C.G. Niu, G.M. Zeng, Novel ternary heterojunction photcocatalyst of Ag nanoparticles and g-C_3N_4 nanosheets co-modified $BiVO_4$ for wider spectrum visible-light photocatalytic degradation of refractory pollutant, Appl. Catal. B Environ. 205 (2017) 133–147.

[44] R.Z. Sun, Q.M. Shi, M. Zhang, L.H. Xie, J.S. Chen, X.M. Yang, M.X. Chen, W. R. Zhao, Enhanced photocatalytic oxidation of toluene with a coral-like direct Z-scheme $BiVO_4$/g-C_3N_4 photocatalyst, J. Alloys Compd. 714 (2017) 619–626.

[45] J. Zhao, J.H. Yan, H.J. Jia, S.W. Zhong, X.Y. Zhang, L. Xu, $BiVO_4$/g-C_3N_4 composite visible-light photocatalyst for effective elimination of aqueous organic pollutants, J. Mol. Catal. 424 (2016) 162–170.

[46] S.A. Ansari, Z. Khan, M.O. Ansari, M.H. Cho, Earth-abundant stable elemental semiconductor red phosphorus-based hybrids for environmental remediation and energy storage applications, RSC Adv. 6 (2016) 44616–44629.